THE JOURNAL OF PHYSICAL CHEMISTRY C

Article

Cite This: J. Phys. Chem. C 2017, 121, 23268-23275

pubs.acs.org/JPCC

Atomistic Simulation Protocol for Improved Design of Si−O−C Hybrid Nanostructures as Li-Ion Battery Anodes: ReaxFF Reactive Force Field

Byung Chul Yeo,[†,‡,∥] Hyun Jung,[†,∥] Hong Woo Lee,[§] Kang-Seop Yun,[†] Hyungjun Kim,[‡] Kwang-Ryeol Lee,[†] and Sang Soo Han*[,†]

[†]Computational Science Research Center, Korea Institute of Science and Technology (KIST), 5 Hwarangno 14-gil, Seongbuk-gu, Seoul 02792, Republic of Korea

[‡]School of Electrical and Electronic Engineering, Yonsei University, Seoul 03722, Republic of Korea

[§]Department of Organic Material Science and Engineering, Pusan National University, Busan 46241, Republic of Korea

Supporting Information

ABSTRACT: Recently, silicon−oxygen−carbon hybrid nanostructures have received great attention as a promising anode material for Li-ion batteries, for which their diverse structures can be synthesized. Here, using molecular dynamics (MD) simulations with a reactive force field (ReaxFF), we studied the atomistic lithiation behaviors of sp^2 carbon-coated Si and SiO_x nanostructures, such as nanowires (NWs) and nanoparticles (NPs), in which various kinds and sizes of carbonaceous coating layers were explored. The introduction of an sp^2 carbonaceous coating layer to Si-based anodes makes Li diffusion more facile, which leads to improved battery performances such as faster charge/discharge rates. Moreover, the carbonaceous coating layer can also provide a buffer effect to volume changes during lithiation along with the well-known functions of preventing the loss of electrical continuity and increasing electrical conductivity of Si-based anodes. However, a thick carbonaceous coating layer can strongly suppress the volume expansion behavior of Si-based nanostructures and thus prevent Li penetration into the nanostructures, leading to a very low Li capacity. According to our ReaxFF-MD simulations, the critical size of the carbonaceous coating layer that can act as a buffer layer is approximately C/Si = 2.4, which is the circumference ratio of the carbonaceous coating layer over the Si NWs. For a coating layer that has a higher ratio, Li cannot penetrate into the Si NWs; instead, they exist only on and in the sp^2 coating layers including in the spaces between two graphene layers. Moreover, the shape of the Si nanostructures (e.g., NW and NP) does little to affect the anode properties, such as Li capacity and volume change, although Si NP confined in a carbon nanotube shows anisotropic volume expansion behavior during lithiation. We expect that the ReaxFF will provide a useful protocol for designing Si−O−C hybrid anodes to obtain better performing Li-ion batteries.

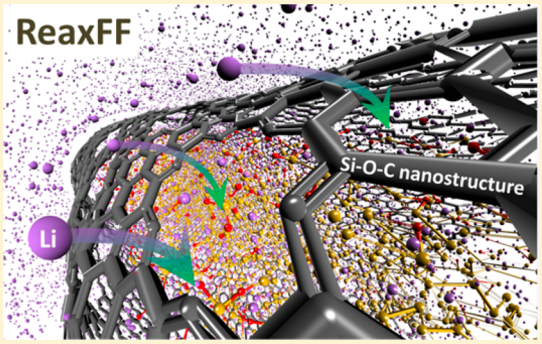

1. INTRODUCTION

Silicon (Si) is one of the most promising and widely investigated candidates as a next generation anode material for Li-ion batteries (LIBs) because of its high Li capacity and abundance.[1−4] However, the large volume fluctuation during the lithiation/delithiation process leads to fracturing of the material followed by rapid capacity fading due to the loss of electrical continuity.[1,5,6] For strategies to overcome the drawbacks of Si, several approaches, such as nanosized structures,[7−13] silicon suboxides (SiO_x),[14−32] and silicon−carbon composites,[33−36] have been investigated. In particular, a combination of Si with carbonaceous materials such as graphite,[33] graphene,[35,36] and carbon nanotube (CNT),[27] has improved the cyclic stability in which carbon provides an enhanced buffering effect and electrical conductivity. Moreover, Si@SiO_x@C nanocomposites with a core−shell structure have demonstrated significantly improved battery performances, such as high reversible capacity, excellent cyclability, and high rate capability.[37,38] Thus, the development of novel Si−O−C hybrid nanostructures is of great significance for LIBs.

In developing such anode materials, understanding of the atomistic lithiation mechanism using computer simulations can provide remarkably valuable information. Of the various computational methods, a reactive force field (ReaxFF) can act as a sweet spot for this type of study because chemical reactions between atoms in real nanosized systems can be predicted with reasonable accuracy.[39−41] Indeed, we previously clarified atomistic lithiation mechanisms of pristine Si and SiO_x nanowires (NWs) with diameters of approximately 5 nm and lengths of approximately 10 nm using molecular dynamics

Received: July 18, 2017
Revised: September 7, 2017
Published: October 9, 2017

DOI: 10.1021/acs.jpcc.7b07095
J. Phys. Chem. C 2017, 121, 23268−23275

(MD) simulations that employ this developed ReaxFF method.[42,43] In particular, a ReaxFF-MD simulation study showed that the anisotropic volume expansion behavior of Si NWs during lithiation relies on the surface structures of Si NWs,[42] which was supported by an experiment.[44,45] However, the volumes of fully lithiated Si NWs are almost identical irrespective of the surface structures. Moreover, in the ReaxFF-MD simulation,[42] we observed the transient formation of silicene-like structures in the Si NWs.[46] Independently, several research groups also reported ReaxFF studies on Si-based anodes for LIBs.[47−53]

In this regard, ReaxFF is definitely useful in predicting anode properties (Li capacity, volume change, Li diffusivity, etc.) of the Si−O−C hybrid nanostructures and for unraveling their lithiation mechanisms. In this work, using the ReaxFF method that we recently developed via first-principles calculations, we report the atomistic lithiation behaviors of carbon-coated Si and SiO_x nanostructures, such as NWs and nanoparticles (NPs), in which various kinds and sizes of the carbon coating layers were considered.

2. COMPUTATIONAL DETAILS

To simulate the lithiation behavior of the Si−O−C hybrid nanostructures (NW and NPs) at the atomic level, we used an MD simulation employing ReaxFF. Very recently, we developed ReaxFF[54] for the Si−Li−O−C−H−F system based on our previous ReaxFF for Si−Li[42] and Si−Li−O[43] systems, with which we successfully simulated the formation of the solid−electrolyte interphase on Si-based anodes. In the work, while developing the ReaxFF parameters for Si−C and C−Li pairs on the basis of our previous Si−Li−O ReaxFF, we considered various relevant trainsets: equation of states (EOSs) of various Si−C crystals, bond dissociations of C−Si single and double bonds in relevant clusters ($H_3C—SiH_3$ and $H_2C═SiH_2$), bond dissociations of the C—Li σ bond in C_6H_5Li, and dispersion interactions between Li and graphene. Thus, the ReaxFF for the Si−Li−O−C−H−F system is applicable for lithiation in the Si−O−C hybrid nanostructures studied in this work.

The MD simulations were performed using LAMMPS software[55] on the iBat simulation platform (http://battery.vfab.org) for LIBs, which was recently developed by our research group. To integrate Newton's equations of motion during the MD simulations, a Verlet algorithm[56] was used with a time step of 0.5 fs (fs). All calculations were performed in a canonical NVT ensemble at 300 K, in which the temperature was maintained using a Nosé−Hoover thermostat[57] with a damping parameter of 0.01 fs^{-1}.

As the Si−O−C hybrid anodes in this work, two nanostructure-type (NWs and NPs) Si-based anodes (Si and SiO_x) were considered along with CNT or graphene-coated layers. Here, the Si NWs have a diameter of 3 nm and a length of 10 nm, and the NPs have a diameter of 3 nm. For the SiO_x NWs and NPs, we obtained the SiO_x materials through chemical reactions between O_2 molecules and pristine Si materials that were simulated using the ReaxFF-MD simulations, which are similar to our previous simulation.[43] The obtained SiO_x has a composition of $SiO_{0.43}$ with a Si@SiO_2 core@shell structure.

For the lithiation simulation of the Si−O−C hybrid nanostructures, a method was applied that is similar to that used in our previous works[42,43] to investigate the lithiation of Si and $SiO_{0.43}$ NWs. The Si−O−C nanostructures were immersed in a simulation cell with dimensions of 100 Å × 100 Å × 97.8 Å that was filled with Li atoms, and any Li atoms that overlapped the nanostructures were removed, as represented in Figure S1 of the Supporting Information (SI). The total number of atoms in the system was approximately 45 000. Additionally, periodic boundary conditions in the *x*-, *y*-, and *z*-directions were applied during the MD simulations, in which the NW axis is in the *z*-direction, leading to lithiation of the NWs along the *x*- and *y*-directions, although lithiation of the NPs allows all directions.

For penetration of a hexagon ring of carbon in CNTs or graphene, an extremely high energy barrier (10.2 eV) is required,[58] which hardly allows Li penetration through the hexagon ring. However, the penetration can be facilitated by carbon vacancies. According to our density functional theory (DFT) calculations (Figure S2), the mono-, di-, tetra-, and hexavacancies significantly lower the penetration barrier to 2.30, 0.31, 0.02, and 0.01 eV, respectively. Here, the energy barriers for mono- and divacancies are similar to the reported DFT results.[59] Although the ReaxFF slightly overestimates the Li penetration barriers in comparison with the DFT-D2, it reasonably predicts the tendency. Therefore, in this work, we introduced hexavacancies in the CNT or graphene coating layers to induce effective penetration of the coating layers. In addition, in building the Si or $SiO_{0.43}$ materials in CNTs, the optimum distances between the CNT and the Si-based material were determined by the ReaxFF, as represented in Figure S3.

3. RESULTS AND DISCUSSION

3.1. Prediction of the Lithiation Behaviors of Various Si−O−C Hybrid Nanostructures. The lithiation behaviors of various Si−O−C NWs that were obtained from the ReaxFF-MD simulations are shown in Figure 1, along with their Li capacities and volume changes. Here, the Si and $SiO_{0.43}$ NWs

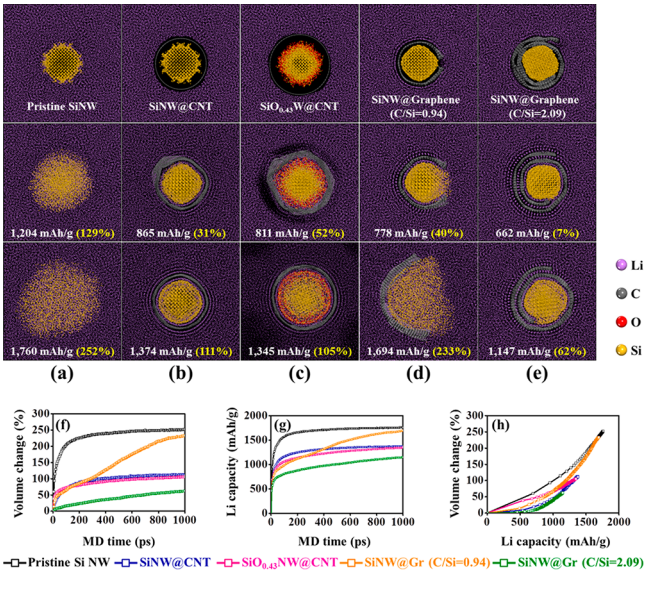

Figure 1. (a−e) ReaxFF-MD snapshots for the lithiation processes of various Si−O−C hybrid nanostructures: (a) pristine Si NW, (b) SiNW@CNT, (c) $SiO_{0.43}$NW@CNT, and (d, e) SiNW@graphene. Here, the top, middle, and bottom figures represent the MD results at 0, 20, and 1000 ps, respectively. (f) Volume changes and (g) Li capacity profiles of various Si−O−C hybrid nanostructures during lithiation, as obtained from the simulations presented in parts a−e. (h) Plot of the volume change versus Li capacity.

DOI: 10.1021/acs.jpcc.7b07095
J. Phys. Chem. C 2017, 121, 23268−23275

with CNT and graphene coating layers are considered, and the behavior of a pristine Si NW with no carbonaceous layer is also presented for comparison. The carbonaceous coating layers include carbon vacancies of 5% for efficient layer penetration of Li. Additionally, for the graphene layers, we considered two different sizes: One has exposed Si atoms that are not completely covered by the graphene layer (Figure 1d), and the second has a Li diffusion channel between two graphene layers (Figure 1e), although all Si atoms are covered by the graphene layer. The carbon edges of the graphene covalently bond to Si, as observed in a prior experiment.[36] Here, the Si−O−C hybrid nanocomposites considered in this work could indeed be synthesized.[27,35,36]

After 1000 picoseconds (ps) of lithiation, the pristine Si NWs had a volume expansion of 252% with a Li capacity of 1760 mAh/g ($Li_{3.38}Si$). However, the Si NWs with the CNT coating (SiNW@CNT) had a volume expansion of 111% and a Li capacity of 1374 mAh/g ($Li_{2.28}Si$), and the $SiO_{0.43}$ NWs with the CNT coating ($SiO_{0.43}$NW@CNT) had a volume expansion of 105% and a Li capacity of 1345 mAh/g ($Li_{1.88}Si$). In Figure 1h, it is apparent that both the Si and $SiO_{0.43}$ NWs coated with CNTs exhibit a smaller volume expansion behavior than that of pristine Si NWs at a given Li concentration, which clearly shows that the CNT coating layer provides a buffer effect on volume expansion of the Si or $SiO_{0.43}$ NWs during lithiation.

For Si NWs coated with graphene (SiNW@graphene), we explored the effects of the graphene size on the lithiation behavior in which the two circumference ratios of graphene over the Si NW (C/Si = 0.94 and 2.09) were considered (Figure 1d,e). The SiNW@graphene composite with a ratio of C/Si = 0.94 shows a similar trend (volume expansion of 233% and a Li capacity of 1694 mAh/g ($Li_{3.26}Si$) at 1000 ps) as the Si NW with no graphene layer, although the graphene provides an effect as a buffer layer on volume expansion during lithiation in the early stage of lithiation (Figure 1h). However, the Si NW@graphene with C/Si = 2.09 shows a smaller amount of lithiation, followed by a smaller volume expansion (volume expansion of 62% for a Li capacity of 1147 mAh/g ($Li_{1.84}Si$) after 1000 ps of lithiation). From these results, the thick carbonaceous coating prevents the efficient lithiation of Si, implying that an appropriate thickness or size of the carbonaceous layer for a given Si nanostructure would exist, which plays a role in the buffer layer for volume expansion and does not simultaneously seriously prevent the lithiation behavior.

In Figure 1h, compared to the pristine Si NW, the SiNW@CNT shows a smaller volume change at a given Li capacity than the pristine Si NW in the early stage of lithiation, although the SiNW@CNT and pristine Si NWs eventually show a similar Li capacity after lithiation of 1000 ps. This indicates that the early stage of lithiation occurs mainly on the CNT layer rather than in the Si bulk. The SiNW@graphene shows a trend similar to that of the SiNW@CNT. However, the SiNW@graphene with a C/Si = 2.09 shows a longer incubation time for the volume expansion and a smaller Li capacity than the composite with C/Si = 0.94. Because the SiNW@graphene with C/Si = 2.09 is a longer graphene layer, it can store relatively more Li on and in the graphene layer than the composite with C/Si = 0.94 and, in particular, between two graphene sheets. Moreover, after lithiation of 1000 ps, the $SiO_{0.43}$NW@CNT shows a smaller volume expansion than the SiNW@CNT because the surface silicon oxide layer can act as a buffer for the volume expansion on the lithiation along with the CNT layer. However, in the early lithiation, the $SiO_{0.43}$NW@CNT has a higher volume expansion because Li preferentially interacts with $SiO_{0.43}$ NW rather than with the CNT layer, in contrast to the case of SiNW@CNT. The detailed lithiation mechanism will be discussed in Section 3.3.

In addition, we investigated the effects of the vacancy concentrations in the CNT layer on the lithiation behaviors of the Si nanostructures. As shown in Figure S4, a higher vacancy concentration leads to a faster lithiation; however, the slopes for volume change versus Li concentration are almost similar, irrespective of the vacancy concentration.

3.2. Effects of Sizes of the Carbonaceous Layers on the Lithiation Behaviors. Intrinsically, Si anodes own the volume expansion characteristics during the interaction with Li, which reveals that a strong suppression of the carbonaceous layers for the volume expansion leads to a low lithiation capacity. Therefore, it is important to find an appropriate size for the layer to buffer the significant volume change of the Si anodes without leading to a serious sacrifice of the Li capacity.

Figure 2 shows the lithiation behaviors of SiNW@graphene composites, where various sizes of graphene layers (i.e., C/Si

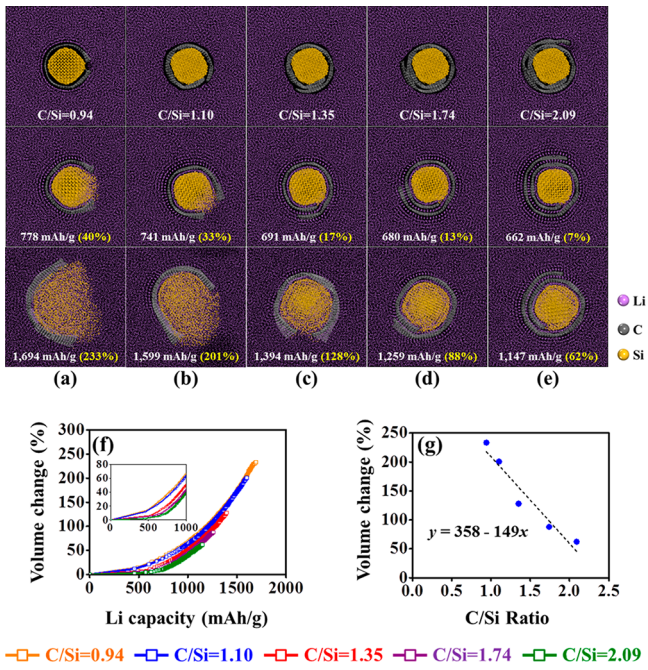

Figure 2. (a−e) ReaxFF-MD snapshots for the lithiation processes of SiNW@graphene composites with various graphene sizes (C/Si ratio): (a) C/Si = 0.94, (b) C/Si = 1.10, (c) C/Si = 1.35, (d) C/Si = 1.74, and (e) C/Si = 2.09. Here, the top, middle, and bottom figures represent the MD results at 0, 20, and 1000 ps, respectively. (f) Plot of the volume change versus Li capacity, as obtained from the simulations presented in parts a−e. (g) Plot of the volume change versus the C/Si ratio.

ratio = 0.94, 1.10, 1.35, 1.74, and 2.09) were considered. The lithiation behaviors, such as Li capacity and volume change, are dependent on the graphene size. As the graphene size increases (the thickness of the carbonaceous coating layer increases), both the volume expansion degree and the Li capacity decrease. Indeed, at 1000 ps of lithiation, the Li capacities in the SiNW@graphene composites show 1694 mAh/g ($Li_{3.26}Si$) for C/Si = 0.94, 1599 mAh/g ($Li_{2.68}Si$) for 1.10, 1394 mAh/g ($Li_{2.52}Si$) for 1.35, 1259 mAh/g ($Li_{2.13}Si$) for 1.74, and 1147 mAh/g

DOI: 10.1021/acs.jpcc.7b07095
J. Phys. Chem. C 2017, 121, 23268−23275

($Li_{1.84}Si$) for 2.09, and their volume expansion is 233% for C/Si = 0.94, 201% for 1.10, 128% for 1.35, 88% for 1.74, and 62% for 2.09. Using these values, we also investigated the correlations for the volume change versus the graphene size (C/Si ratio), which is shown in Figure 2g. Using the extrapolation of the correlation, we found that when the C/Si ratio is 2.4 the volume change is zero. Thus, for a larger C/Si ratio, Li atoms cannot penetrate into the Si NW. Instead, they exist only on and in graphene layers including the spaces between two graphene layers.

To further explore the constraining effect of the graphene layer, we calculated the von Mises stress distributions of the SiNW@graphene composites in Figure 3, where atomic

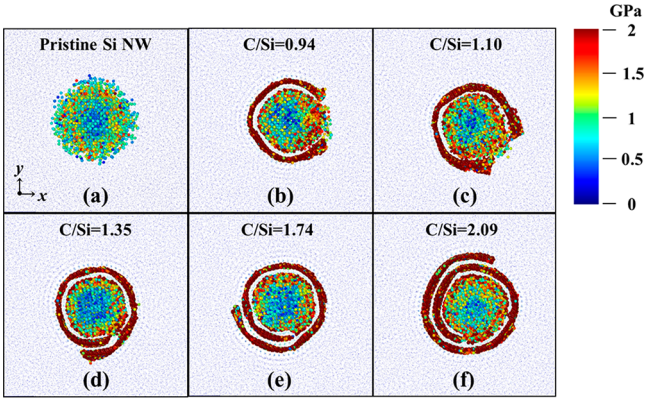

Figure 3. von Mises stresses for lithiated SiNW@graphene composites, where various graphene sizes (C/Si ratio) are considered: (a) pristine Si NW, (b) C/Si = 0.94, (c) C/Si = 1.10, (d) C/Si = 1.35, (e) C/Si = 1.74, and (f) C/Si = 2.09. The stresses are calculated for structures with the same Li capacity (600 mAh/g).

structures at the same Li capacity (600 mAh/g) were considered. The von Mises stress implies one that is required to start yielding or deformation of a material. Additionally, the von Mises stress (σ_v) is calculated according to eq 1:

$$\sigma_v = \sqrt{\frac{1}{2}[(\sigma_{xx} - \sigma_{yy})^2 + (\sigma_{yy} - \sigma_{zz})^2 + (\sigma_{zz} - \sigma_{xx})^2 + 6(\sigma_{xy}^2 + \sigma_{yz}^2 + \sigma_{zx}^2)]} \quad (1)$$

where the σ_{xx}, σ_{yy}, and σ_{zz} are the normal stresses, and the σ_{xy}, σ_{yz}, and σ_{zx} are the shear stresses in an $x-y-z$ coordinate system. Here, the calculated von Mises stress values are similar to the reported experimental lithiation-induced stress values in nanostructured Si anodes by *in situ* measurements.[60,61]

For the pristine Si NW, the Si surface exhibited smaller von Mises stress values than the interior, which indicates that the Si surface is easier to deform due to lithiation. However, for the SiNW@graphene composites, the Si surface near the graphene coating layer has higher von Mises stress values than the core region of the Si NWs. This indicates that the graphene coating leads to a constraint effect for the deformation of the Si surface region, which prevents Li penetration into the Si NW.

We additionally calculated the residual stress distributions of the graphene-coated Si NW (SiNW@graphene) in the radial direction (σ_r) and then compared the results with those for the pristine Si NW, as shown in Figure S22. Here, the residual stress was obtained by averaging the atomic stresses of Si and Li atoms in the concentric shell between r and $r + \delta r$, where r is the radial distance from the center of the NW. The radial stress (σ_r) is calculated using eq 2.[43]

$$\sigma_r = \sigma_{xx} \cos^2\theta + 2\sigma_{xy} \sin\theta\cos\theta + \sigma_{yy} \sin^2\theta \quad (2)$$

Here, the σ_{xx} and σ_{xy} are the normal and shear stresses in an $x-y-z$ coordinate system, respectively, and the θ is an angle.

During the lithiation of a pristine Si NW, the lithiated phase (Li_xSi) has tensile (positive) stresses, which serve as a driving force for the volume expansion of the NW.[43] On the other hand, in the initial SiNW@graphene composite, the Si core is subjected to compressive stresses that are induced by the tensile stresses of the Si−graphene interface. Although the lithiation proceeds, the interface has still tensile stresses and acts as a buffer layer alleviating abrupt changes in stresses. This induces the lithiated Si phase (Li_xSi) to be subjected to compressive stresses, which is in contrast to the pristine Si NW case. Such compressive stresses exerted on the Li_xSi phase induce a retardation effect on the volume expansion of the NW during lithiation. Moreover, the interface also induces compressive stresses to the lithiated graphene layer that is an outmost layer of the NW.

To confirm the constraint effect of carbonaceous coating layers, we performed nudged-elastic band calculations using DFT within the PBE-D2[62] framework to investigate the effects of the carbonaceous layer on the energy barriers for penetration of a Li atom into the Si surface (Figure 4). For a Si(111)

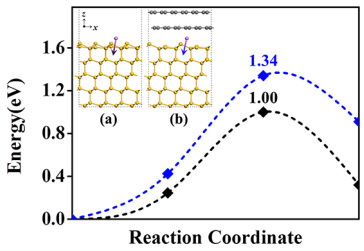

Figure 4. NEB calculations for Li penetration barriers (surface to subsurface) into (a) pristine Si(111) (black) and (b) two-layer graphene-coated Si(111) (blue).

surface with no graphene coating layer, the energy barrier is 1.00 eV, which is similar to the previous DFT calculation.[63] However, the graphene coating increases the energy barrier due to the constraint effect of the coating layers. Indeed, for Si(111) surfaces with two graphene layers, the energy barrier is increased by 1.34 eV, which clearly shows the constraint effect of the graphene layers for Li penetration. According to the analysis (Table S1) of the DFT stress tensor components for the initial structures of Figure 4, σ_{zz} in the pristine Si is 0.57 kbar (tensile stress), while σ_{zz} in the two-layer graphene-coated Si is −5.04 kbar (compressive stress). Here, we focus on the stress tensor component along the z-direction because the Li insertion into the Si bulk proceeds along the direction. Indeed, the carbon coating layer can induce a compressive strain effect, which leads to a higher Li penetration barrier. In addition, we need to mention that the current ReaxFF provides the Li penetration barrier similar to that of the DFT (DFT 1.34 eV vs ReaxFF 1.31 eV).

To validate prediction of atomic charges by the ReaxFF, we compare the ReaxFF values with the DFT ones, as shown in Figure S23a. For the structure shown in Figure 4b, the ReaxFF predicts very similar atomic charges for Si and C atoms to those of DFT, although the ReaxFF tends to underestimate atomic

DOI: 10.1021/acs.jpcc.7b07095
J. Phys. Chem. C 2017, 121, 23268−23275

charges of Li atoms. Therefore, the present ReaxFF can reasonably predict atomic charges in various carbon-coated Si hybrid nanostructures. We have also investigated effects of sizes of the carbon coating layers on atomic charge distribution in graphene-coated Si NWs in Figure S23b–f. Our ReaxFF simulations reveal that the effect of the graphene coating size is not significant, which implies that the NWs have similar driving forces for the lithiation process.

Thus far, we have focused on the lithiation behavior of Si or $SiO_{0.43}$ NWs with carbonaceous coating layers. As shown in Figure 5, we additionally investigated the lithiation behaviors of

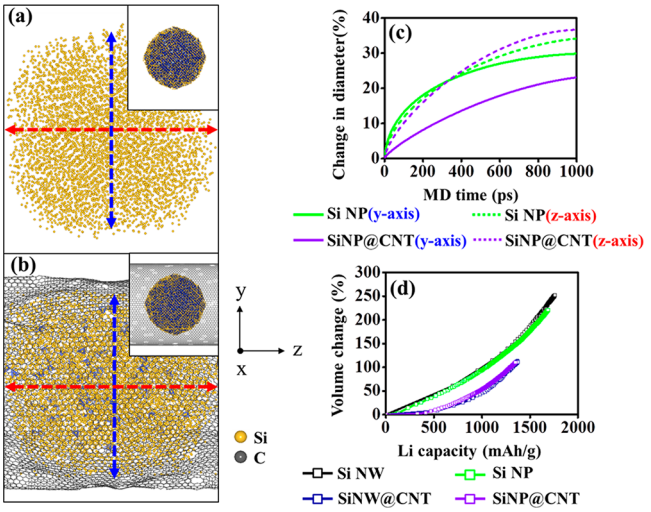

Figure 5. ReaxFF-MD snapshots for the spherical Si NP (a) and SiNP@CNT composite (b) at 1000 ps, where the insets indicate each initial structure. (c) Their volume expansion along the *y*- and *z*-directions, where the CNT axis is the *z*-direction. (d) Comparison of volume change versus Li capacity of the Si NPs and Si NWs.

spherical Si NPs in CNTs, which can be experimentally synthesized.[27] Spherical Si NPs without the CNT coating show uniform volume expansion during lithiation. However, the CNT coating leads to anisotropic volume expansion of the Si NP in which the volume expansion behavior along the axis direction of the CNT is more feasible because the Si NP is under constraint along the radial direction by the CNT layer. Moreover, we observed that the shape of Si nanostructures (e.g., NW and NP) does little to affect the anode properties, such as Li capacity and volume change (Figure 5d).

It was reported that an anisotropic volume expansion during the lithiation of Si NWs occurred due to the different levels of expansion along different crystallographic orientations.[64] Here, largely incompatible strains are generated at the intersections of adjacent crystalline (110) facets near the outer surface, leading to surface crack nucleation at well-defined angular sites. Although we have observed such an anisotropic volume expansion in the CNT-coated Si NP, the surface crack nucleation induced by the phenomenon has not been found, which is probably due to the time limit of MD simulations.

3.3. Lithiation Mechanisms of Si and SiO_x Nanostructures Coated with Carbonaceous Layers. To clarify the lithiation mechanism of Si or $SiO_{0.43}$ NWs coated with carbonaceous layers, we scrutinized the MD trajectories for Si and $SiO_{0.43}$ NWs coated with CNT layers, which is shown in Figure 6. For pristine Si NWs, Li atoms interact with Si surfaces, and amorphous Li_xSi phases are generated in which

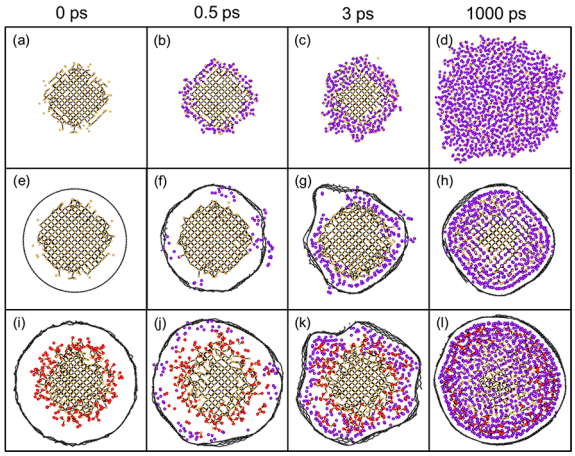

Figure 6. Comparison of the lithiation mechanisms for (a–d) pristine Si, (e–h) SiNW@CNT, and (i–l) $SiO_{0.43}$NW@CNT. Color codes for atoms are yellow = Si, gray = C, red = O, and purple = Li. Here, most Li atoms are removed for clarity.

lithiation proceeds uniformly (Figure 6a). Detailed information on the lithiation mechanism can be found in our previous work.[42] However, in the SiNW@CNT composite (Figure 6b), Li atoms penetrating through carbon vacancies in the CNT layer tend to preferentially diffuse at the interface between the CNT layer and Si surface rather than penetrate into the Si surface. However, for the $SiO_{0.43}$NW@CNT composite (Figure 6c), the Li atoms penetrating through the defects in the CNT interact with oxygen atoms in $SiO_{0.43}$, leading to the evolution of Li_2O and Li_4SiO_4, as reported in our previous study.[43] Simultaneously, Li atoms that do not interact with the oxygen atom preferentially diffuse into the interface between the CNT layer and the $SiO_{0.43}$ surface rather than penetrate into the interior of the $SiO_{0.43}$ NW, as similarly observed in the SiNW@CNT.

From the SiNW@CNT result, it can be expected that the interfacial diffusion of Li is more facile than bulk diffusion in the Si. We also calculated the mean-square displacements from the MD trajectories for the interfacial and bulk diffusion of Li atoms, as shown in Figure 7. Indeed, the interfacial diffusivity is

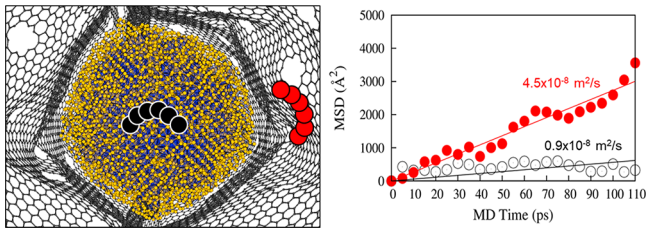

Figure 7. Mean-squared displacements for Li diffusions at the interface between Si NWs and CNTs (red) and inside the Si bulk (black).

approximately 5 times higher than the bulk diffusivity (4.5×10^{-8} m^2/s vs 0.9×10^{-8} m^2/s) because the sp^2 carbon provides a slide effect of Li diffusion. A similar result was also reported in the previous first-principles MD work.[65] This is also supported by a recent experimental measurement that showed that Li diffusion is extremely fast in bilayer graphene.[66] In the *c*-Si bulk, a Li atom diffuses from one tetrahedral interstitial site into another interstitial site.[67] At each interstitial site, one Li atom interacts with six Si atoms. On the other hand, in the case of the interfacial diffusion between Si surface and graphene, one Li

DOI: 10.1021/acs.jpcc.7b07095
J. Phys. Chem. C 2017, 121, 23268–23275

atom interacts with three Si atoms. Of course, the Li atom also interacts with carbon atoms in graphene. Moreover, the Li diffusion channel size at the interface is bigger than that in the *c*-Si bulk. In Figure 4b, the Si−Si (covalent bonding) bond distance in the Si bulk and the Si−C (nonbonded interaction) distance at the interface along *z*-direction are 2.4 and 3.5 Å, respectively. The bigger diffusion channel at the interface results from delocalization stability of electron in the sp^2 carbon and then leads to facile diffusion of Li atoms. Using NEB calculations within the DFT framework, we additionally compared Li diffusion barriers in the *c*-Si bulk and at the interface, where the structure of Figure 4b was considered. Indeed, our DFT calculations reveal that the Li diffusion barrier in the *c*-Si bulk is higher (0.5 eV vs 0.2 eV), which supports our ReaxFF-MD simulation.

As a result, introduction of the sp^2 carbonaceous coating layer into Si-based anodes makes Li diffusion more facile, which leads to improved battery performances, such as faster charge/discharge rates. Of course, the carbon coating layer can also provide a buffer effect to volume changes during lithiation, along with preventing the loss of electrical continuity and increasing the electrical conductivity of the Si-based anodes.

4. SUMMARY AND CONCLUSION

Using MD simulations with ReaxFF, we can predict anode properties (e.g., Li capacities and volume changes) of various Si−O−C hybrid nanostructures for LIBs and understand the effects of carbonaceous coating layers on the anode properties. It has been typically believed that a significant volume expansion of Si anodes during lithiation can be prevented by the carbonaceous coating layer, leading to improved battery performance. Although the carbonaceous layer can provide a buffer effect on the volume expansion, the thick layer can also suppress Li penetration into the Si anode, which leads to a very low Li capacity. According to our ReaxFF-MD simulation, for a carbonaceous coating layer with a C/Si ratio of greater than 2.4, Li atoms cannot penetrate into the Si NW. Instead, they exist only on and in graphene layers including in spaces between two graphene layers.

In addition, a sp^2 carbonaceous coating layer can provide a facile Li diffusion channel along the interfaces between the carbon coating layer and the Si nanostructures, which leads to faster charge/discharge rates. Therefore, in CNT or graphene-coated Si-based anodes, Li atoms penetrating through the carbonaceous coating layer tend to diffuse preferentially on the interface between the layer and Si surface. After full coverage of Li on the interface, Li atoms begin to penetrate into the interior of the Si nanostructures. From these results, we expect that the ReaxFF will provide a useful protocol for designing Si−O−C hybrid anodes to obtain better performing LIBs.

■ ASSOCIATED CONTENT

Supporting Information

The Supporting Information is available free of charge on the ACS Publications website at DOI: 10.1021/acs.jpcc.7b07095.

Computational details and additional ReaxFF-MD results regarding lithiation of the Si−O−C hybrid nanostructures (PDF)

■ AUTHOR INFORMATION

Corresponding Author

*E-mail: sangsoo@kist.re.kr. Phone: +82 2 958 5441. Fax: +82 2 958 5451.

ORCID

Sang Soo Han: 0000-0002-7925-8105

Author Contributions

‖B.C.Y. and H.J. contributed equally to this work.

Notes

The authors declare no competing financial interest.

■ ACKNOWLEDGMENTS

We acknowledge the financial support from the Korea Institute of Science and Technology (Grants 2E26940 and 2E27090) and from the Industrial Strategic Technology Development Program (Grant 10041589) funded by the Ministry of Trade, Industry, and Energy (MOTIE) of Korea. This work was also supported by the National Research Foundation of Korea Grant funded by the Korean Government (MSIP) (NRF-2011-C1AA001-0030538).

■ REFERENCES

(1) Kasavajjula, U.; Wang, C.; Appleby, A. J. Nano- and Bulk-Silicon-Based Insertion Anodes for Lithium-Ion Secondary Cells. *J. Power Sources* **2007**, *163*, 1003−1039.

(2) Obrovac, M. N.; Christensen, L. Structural Changes in Silicon Anodes during Lithium Insertion/Extraction. *Electrochem. Solid-State Lett.* **2004**, *7*, A93−A96.

(3) Obrovac, M. N.; Krause, L. J. Reversible Cycling of Crystalline Silicon Powder. *J. Electrochem. Soc.* **2007**, *154*, A103−A108.

(4) Liu, X. H.; Zheng, H.; Zhong, L.; Huang, S.; Karki, K.; Zhang, L. Q.; Liu, Y.; Kushima, A.; Liang, W. T.; Wang, J. W.; et al. Anisotropic Swelling and Fracture of Silicon Nanowires during Lithiation. *Nano Lett.* **2011**, *11*, 3312−3318.

(5) Larcher, D.; Beattie, S.; Morcrette, M.; Edström, K.; Jumas, J.-C.; Tarascon, J.-M. Recent Findings and Prospects in the Field of Pure Metals as Negative Electrodes for Li-Ion Batteries. *J. Mater. Chem.* **2007**, *17*, 3759−3772.

(6) Zhou, S.; Liu, X.; Wang, D. Si/$TiSi_2$ Heteronanostructures as High-capacity Anode Material For Li Ion Batteries. *Nano Lett.* **2010**, *10*, 860−863.

(7) Magasinski, A.; Dixon, P.; Hertzberg, B.; Kvit, A.; Ayala, J.; Yushin, G. High-Performance Lithium-Ion Anodes Using a Hierarchical Bottom-up Approach. *Nat. Mater.* **2010**, *9*, 353−358.

(8) Chan, C. K.; Peng, H.; Liu, G.; McIlwrath, K.; Zhang, X. F.; Huggins, R. A.; Cui, Y. High-Performance Lithium Battery Anodes Using Silicon Nanowires. *Nat. Nanotechnol.* **2008**, *3*, 31−35.

(9) Cui, L.-F.; Ruffo, R.; Chan, C. K.; Peng, H.; Cui, Y. Crystalline-Amorphous Core−Shell Silicon Nanowires for High Capacity and High Current Battery Electrodes. *Nano Lett.* **2009**, *9*, 491−495.

(10) Kim, H.; Seo, M.; Park, M. H.; Cho, J. A Critical Size of Silicon Nano-Anodes for Lithium Rechargeable Batteries. *Angew. Chem., Int. Ed.* **2010**, *49*, 2146−2149.

(11) Song, T.; Xia, J.; Lee, J. H.; Lee, D. H.; Kwon, M. S.; Choi, J. M.; Wu, J.; Doo, S. K.; Chang, H.; Park, W. I.; et al. Arrays of Sealed Silicon Nanotubes as Anodes for Lithium Ion Batteries. *Nano Lett.* **2010**, *10*, 1710−1716.

(12) Yu, Y.; Gu, L.; Zhu, C.; Tsukimoto, S.; van Aken, P. A.; Maier, J. Reversible Storage of Lithium in Silver-Coated Three-Dimensional Macroporous Silicon. *Adv. Mater.* **2010**, *22*, 2247−2250.

(13) Park, M. H.; Kim, M. G.; Joo, J.; Kim, K.; Kim, J.; Ahn, S.; Cui, Y.; Cho, J. Silicon Nanotube Battery Anodes. *Nano Lett.* **2009**, *9*, 3844−3847.

(14) Kim, T.; Park, S.; Oh, S. M. Solid-State NMR and Electrochemical Dilatometry Study on Li^+ Uptake/Extraction

Mechanism in SiO Electrode. *J. Electrochem. Soc.* **2007**, *154*, A1112−A1117.
(15) Song, K.; Yoo, S.; Kang, K.; Heo, H.; Kang, Y. M.; Jo, M. H. Hierarchical SiO_x Nanoconifers for Li-Ion Battery Anodes with Structural Stability and Kinetic Enhancement. *J. Power Sources* **2013**, *229*, 229−233.
(16) Nagao, Y.; Sakaguchi, H.; Honda, H.; Fukunaga, T.; Esaka, T. Structural Analysis of Pure and Electrochemically Lithiated SiO Using Neutron Elastic Scattering. *J. Electrochem. Soc.* **2004**, *151*, A1572−A1575.
(17) Chang, W.-S.; Park, C.-M.; Kim, J.-H.; Kim, Y.-U.; Jeong, G.; Sohn, H.-J. Quartz (SiO_2): A New Energy Storage Anode Material for Li-Ion Batteries. *Energy Environ. Sci.* **2012**, *5*, 6895−6899.
(18) Miyachi, M.; Yamamoto, H.; Kawai, H.; Ohta, T.; Shirakata, M. Analysis of SiO Anodes for Lithium-Ion Batteries. *J. Electrochem. Soc.* **2005**, *152*, A2089−A2091.
(19) Abel, P. R.; Lin, Y.-M.; Celio, H.; Heller, A.; Mullins, C. B. Improving the Stability of Nanostructured Silicon Thin Film Lithium-Ion Battery Anodes through Their Controlled Oxidation. *ACS Nano* **2012**, *6*, 2506−2516.
(20) Iacona, F.; Bongiorno, C.; Spinella, C.; Boninelli, S.; Priolo, F. Formation and Evolution of Luminescent Si Nanoclusters Produced by Thermal Annealing of SiO_x Films. *J. Appl. Phys.* **2004**, *95*, 3723−3732.
(21) Wang, Y. Q.; Smirani, R.; Ross, G. G. The Formation Mechanism of Si Nanocrystals in SiO_2. *J. Cryst. Growth* **2006**, *294*, 486−489.
(22) Park, C.-M.; Choi, W.; Hwa, Y.; Kim, J.-H.; Jeong, G.; Sohn, H.-J. Characterizations and Electrochemical Behaviors of Disproportionated SiO and Its Composite for Rechargeable Li-Ion Batteries. *J. Mater. Chem.* **2010**, *20*, 4854−4860.
(23) Mamiya, M.; Takei, H.; Kikuchi, M.; Uyeda, C. Preparation of Fine Silicon Particles from Amorphous Silicon Monoxide by the Disproportionation Reaction. *J. Cryst. Growth* **2001**, *229*, 457−461.
(24) Mamiya, M.; Kikuchi, M.; Takei, H. Crystallization of Fine Silicon Particles from Silicon Monoxide. *J. Cryst. Growth* **2002**, *237*, 1909−1914.
(25) Wu, H.; Chan, G.; Choi, J. W.; Ryu, I.; Yao, Y.; McDowell, M. T.; Lee, S. W.; Jackson, A.; Yang, Y.; Hu, L.; et al. Stable Cycling of Double-Walled Silicon Nanotube Battery Anodes through Solid−electrolyte Interphase Control. *Nat. Nanotechnol.* **2012**, *7*, 310−314.
(26) McDowell, M. T.; Lee, S. W.; Ryu, I.; Wu, H.; Nix, W. D.; Choi, J. W.; Cui, Y. Novel Size and Surface Oxide Effects in Silicon Nanowires as Lithium Battery Anodes. *Nano Lett.* **2011**, *11*, 4018−4025.
(27) Hertzberg, B.; Alexeev, A.; Yushin, G. Deformations in Si-Li Anodes upon Electrochemical Alloying in Nano-Confined Space. *J. Am. Chem. Soc.* **2010**, *132*, 8548−8549.
(28) Favors, Z.; Wang, W.; Bay, H. H.; George, A.; Ozkan, M.; Ozkan, C. S. Stable Cycling of SiO_2 Nanotubes as High-Performance Anodes for Lithium-Ion Batteries. *Sci. Rep.* **2015**, *4*, 4605.
(29) Ban, C.; Kappes, B. B.; Xu, Q.; Engtrakul, C.; Ciobanu, C. V.; Dillon, A. C.; Zhao, Y. Lithiation of Silica through Partial Reduction. *Appl. Phys. Lett.* **2012**, *100*, 243905.
(30) Zhang, Y.; Li, Y.; Wang, Z.; Zhao, K. Lithiation of SiO_2 in Li-Ion Batteries: In Situ Transmission Electron Microscopy Experiments and Theoretical Studies. *Nano Lett.* **2014**, *14*, 7161−7170.
(31) Chou, C. Y.; Hwang, G. S. Lithiation Behavior of Silicon-Rich Oxide ($SiO_{1/3}$): A First-Principles Study. *Chem. Mater.* **2013**, *25*, 3435−3440.
(32) Perez-Beltran, S.; Ramírez-Caballero, G. E.; Balbuena, P. B. First-Principles Calculations of Lithiation of a Hydroxylated Surface of Amorphous Silicon Dioxide. *J. Phys. Chem. C* **2015**, *119*, 16424−16431.
(33) Ng, S. H.; Wang, J.; Wexler, D.; Konstantinov, K.; Guo, Z. P.; Liu, H. K. Highly Reversible Lithium Storage in Spheroidal Carbon-Coated Silicon Nanocomposites as Anodes for Lithium-Ion Batteries. *Angew. Chem., Int. Ed.* **2006**, *45*, 6896−6899.
(34) McDowell, M. T.; Woo Lee, S.; Wang, C.; Cui, Y. The Effect of Metallic Coatings and Crystallinity on the Volume Expansion of Silicon during Electrochemical Lithiation/delithiation. *Nano Energy* **2012**, *1*, 401−410.
(35) Luo, J.; Zhao, X.; Wu, J.; Jang, H. D.; Kung, H. H.; Huang, J. Crumpled Graphene-Encapsulated Si Nanoparticles for Lithium Ion Battery Anodes. *J. Phys. Chem. Lett.* **2012**, *3*, 1824−1829.
(36) Son, I. H.; Hwan Park, J.; Kwon, S.; Park, S.; Rümmeli, M. H.; Bachmatiuk, A.; Song, H. J.; Ku, J.; Choi, J. W.; Choi, J.-M.; et al. Silicon Carbide-Free Graphene Growth on Silicon for Lithium-Ion Battery with High Volumetric Energy Density. *Nat. Commun.* **2015**, *6*, 7393.
(37) Hu, Y.; Demir-cakan, R.; Titirici, M.; Müller, J.; Schlögl, R.; Antonietti, M.; Maier, J. Superior Storage Performance of a $Si@SiO_X$/C Nanocomposite as Anode Material for Lithium-Ion Batteries. *Angew. Chem., Int. Ed.* **2008**, *47*, 1645−1649.
(38) Su, L.; Zhou, Z.; Ren, M. Core Double-Shell $Si@SiO_2@C$ Nanocomposites as Anode Materials for Li-Ion Batteries. *Chem. Commun.* **2010**, *46*, 2590−2592.
(39) van Duin, A. C. T.; Dasgupta, S.; Lorant, F.; Goddard, W. A. ReaxFF: A Reactive Force Field for Hydrocarbons. *J. Phys. Chem. A* **2001**, *105*, 9396−9409.
(40) van Duin, A. C. T.; Strachan, A.; Stewman, S.; Zhang, Q.; Xu, X.; Goddard, W. A., III $ReaxFF_{SiO}$ Reactive Force Field for Silicon and Silicon Oxide Systems. *J. Phys. Chem. A* **2003**, *107*, 3803−3811.
(41) Senftle, T. P.; Hong, S.; Islam, M. M.; Kylasa, S. B.; Zheng, Y.; Shin, Y. K.; Junkermeier, C.; Engel-Herbert, R.; Janik, M. J.; Aktulga, H. M.; et al. The ReaxFF Reactive Force-Field: Development, Applications and Future Directions. *NPJ. Comput. Mater.* **2016**, *2*, 15011.
(42) Jung, H.; Lee, M.; Yeo, B. C.; Lee, K.-R.; Han, S. S. Atomistic Observation of the Lithiation and Delithiation Behaviors of Silicon Nanowires Using Reactive Molecular Dynamics Simulations. *J. Phys. Chem. C* **2015**, *119*, 3447−3455.
(43) Jung, H.; Yeo, B. C.; Lee, K.-R.; Han, S. S. Atomistics of the Lithiation of Oxidized Silicon (SiO_x) Nanowires in Reactive Molecular Dynamics Simulations. *Phys. Chem. Chem. Phys.* **2016**, *18*, 32078−32086.
(44) Lee, S. W.; McDowell, M. T.; Choi, J. W.; Cui, Y. Anomalous Shape Changes of Silicon Nanopillars by Electrochemical Lithiation. *Nano Lett.* **2011**, *11*, 3034−3039.
(45) Lee, S. W.; McDowell, M. T.; Berla, L. A.; Nix, W. D.; Cui, Y. Fracture of Crystalline Silicon Nanopillars during Electrochemical Lithium Insertion. *Proc. Natl. Acad. Sci. U. S. A.* **2012**, *109*, 4080−4085.
(46) Liu, X. H.; Wang, J. W.; Huang, S.; Fan, F.; Huang, X.; Liu, Y.; Krylyuk, S.; Yoo, J.; Dayeh, S. A.; Davydov, A. V.; et al. In Situ Atomic-Scale Imaging of Electrochemical Lithiation in Silicon. *Nat. Nanotechnol.* **2012**, *7*, 749−756.
(47) Fan, F.; Huang, S.; Yang, H.; Raju, M.; Datta, D.; Shenoy, V. B.; van Duin, A. C. T.; Zhang, S.; Zhu, T. Mechanical Properties of Amorphous Li_xSi Alloys: A Reactive Force Field Study. *Modell. Simul. Mater. Sci. Eng.* **2013**, *21*, 074002.
(48) Kim, S.-P.; Datta, D.; Shenoy, V. B. Atomistic Mechanisms of Phase Boundary Evolution during Initial Lithiation of Crystalline Silicon. *J. Phys. Chem. C* **2014**, *118*, 17247−17253.
(49) Ostadhossein, A.; Kim, S. Y.; Cubuk, E. D.; Qi, Y.; Van Duin, A. C. T. Atomic Insight into the Lithium Storage and Diffusion Mechanism of SiO_2/Al_2O_3 Electrodes of Lithium Ion Batteries: ReaxFF Reactive Force Field Modeling. *J. Phys. Chem. A* **2016**, *120*, 2114−2127.
(50) Kim, S.-Y.; Ostadhossein, A.; van Duin, A. C. T.; Xiao, X.; Gao, H.; Qi, Y. Self-Generated Concentration and Modulus Gradient Coating Design to Protect Si Nano-Wire Electrodes during Lithiation. *Phys. Chem. Chem. Phys.* **2016**, *18*, 3706−3715.
(51) Kim, K. J.; Wortman, J.; Kim, S.-Y.; Qi, Y. Atomistic Simulation Derived Insight on the Irreversible Structural Changes of Si Electrode during Fast and Slow Delithiation. *Nano Lett.* **2017**, *17*, 4330−4338.
(52) Ostadhossein, A.; Cubuk, E. D.; Tritsaris, G. A.; Kaxiras, E.; Zhang, S.; van Duin, A. C. T. Stress Effects on the Initial Lithiation of

DOI: 10.1021/acs.jpcc.7b07095
J. Phys. Chem. C 2017, 121, 23268−23275

Crystalline Silicon Nanowires: Reactive Molecular Dynamics Simulations Using ReaxFF. *Phys. Chem. Chem. Phys.* **2015**, *17*, 3832−3840.
(53) Ding, B.; Wu, H.; Xu, Z.; Li, X.; Gao, H. Stress Effects on Lithiation in Silicon. *Nano Energy* **2017**, *38*, 486−493.
(54) Yun, K.-S.; Pai, S. J.; Yeo, B. C.; Lee, K.-R.; Kim, S.-J.; Han, S. S. Simulation Protocol for Prediction of a Solid-Electrolyte Interphase on the Silicon-Based Anodes of a Lithium-Ion Battery: ReaxFF Reactive Force Field. *J. Phys. Chem. Lett.* **2017**, *8*, 2812−2818.
(55) Plimpton, S. Fast Parallel Algorithms for Short-Range Molecular Dynamics. *J. Comput. Phys.* **1995**, *117*, 1−19.
(56) Verlet, L. Computer "Experiments" on Classical Fluids. I. Thermodynamical Properties of Lennard-Jones Molecules. *Phys. Rev.* **1967**, *159*, 98−103.
(57) Hoover, W. G. Canonical Dynamics: Equilibrium Phase-Space Distributions. *Phys. Rev. A: At., Mol., Opt. Phys.* **1985**, *31*, 1695−1697.
(58) Yao, F.; Güneş, F.; Ta, H. Q.; Lee, S. M.; Chae, S. J.; Sheem, K. Y.; Cojocaru, C. S.; Xie, S. S.; Lee, Y. H. Diffusion Mechanism of Lithium Ion through Basal Plane of Layered Graphene. *J. Am. Chem. Soc.* **2012**, *134*, 8646−8654.
(59) Fan, X.; Zheng, W. T.; Kuo, J.-L. Adsorption and Diffusion of Li on Pristine and Defective Graphene. *ACS Appl. Mater. Interfaces* **2012**, *4*, 2432−2438.
(60) Zeng, Z.; Liu, N.; Zeng, Q.; Lee, S. W.; Mao, W. L.; Cui, Y. In Situ Measurement of Lithiation-Induced Stress in Silicon Nanoparticles Using Micro-Raman Spectroscopy. *Nano Energy* **2016**, *22*, 105−110.
(61) Kushima, A.; Huang, J. Y.; Li, J. Quantitative Fracture Strength and Plasticity Measurements of Lithiated Silicon Nanowires by In Situ TEM Tensile Experiments. *ACS Nano* **2012**, *6*, 9425−9432.
(62) Grimme, S.; Antony, J.; Ehrlich, S.; Krieg, H. A Consistent and Accurate Ab Initio Parametrization of Density Functional Dispersion Correction (DFT-D) for the 94 Elements H-Pu. *J. Chem. Phys.* **2010**, *132*, 154104.
(63) Jung, S. C.; Han, Y.-K. Facet-Dependent Lithium Intercalation into Si Crystals: Si(100) vs. Si(111). *Phys. Chem. Chem. Phys.* **2011**, *13*, 21282−21287.
(64) Zhang, S. Chemomechanical Modeling of Lithiation-Induced Failure in High-Volume-Change Electrode Materials for Lithium Ion Batteries. *NPJ. Comput. Mater.* **2017**, *3*, 7.
(65) Chou, C.; Hwang, G. S. Role of Interface in the Lithiation of Silicon-Graphene Composites: A First Principles Study. *J. Phys. Chem. C* **2013**, *117*, 9598−9604.
(66) Kühne, M.; Paolucci, F.; Popovic, J.; Ostrovsky, P. M.; Maier, J.; Smet, J. H. Ultrafast Lithium Diffusion in Bilayer Graphene. *Nat. Nanotechnol.* **2017**, *12*, 895.
(67) Kim, H.; Kweon, K. E.; Chou, C.-Y.; Ekerdt, J. G.; Hwang, G. S. On the Nature and Behavior of Li Atoms in Si: A First Principles Study. *J. Phys. Chem. C* **2010**, *114*, 17942−17946.

DOI: 10.1021/acs.jpcc.7b07095
J. Phys. Chem. C 2017, 121, 23268−23275